Journal of Inorganic and Organometallic Polymers and Materials (2024) 34:1081–1091
https://doi.org/10.1007/s10904-023-02861-z

RESEARCH

Heteronuclear Hexacyanometallate(III) Coordination Polymers (Cd/Cr, Cd/Fe, Cd/Co) with 3-(Aminomethyl)pyridine: Synthesis, Characterization, and Catalytic Activities for the Peroxidative Oxidation of Benzylic Alcohols

Seray Kekeç[1] · Güneş Süheyla Kürkçüoğlu[1] · Hakan Ünver[2] · Onur Şahin[3] · Okan Zafer Yeşilel[4]

Received: 28 July 2023 / Accepted: 5 September 2023 / Published online: 4 October 2023

Abstract
Three new heteronuclear hexacyanometallate(III) coordination polymers (CPs), $[Cd_3(\mu\text{-}3ampy)_4(H_2O)_4Cr_2(\mu\text{-}CN)_8(CN)_4]_n$ (**1**), $[Cd_3(\mu\text{-}3ampy)_2(H_2O)_2Fe_2(\mu\text{-}CN)_5(CN)_7]_n$ (**2**) and $[Cd_3(\mu\text{-}3ampy)_4(H_2O)_4Co_2(\mu\text{-}CN)_8(CN)_4]_n$ (**3**), were synthesized with 3-(aminomethyl)pyridine (3ampy) ligand. All CPs were characterized by FT-IR, Raman, elemental, thermal analysis as well as single crystal X-ray diffraction and powder X-ray diffraction techniques. The single crystal X-ray diffraction analyses shows that the CPs **1** and **3** are two-dimensional structures, whereas CP **2** is a three-dimensional structure where two adjacent metal ions ions are linked via 3ampy and CN bridges. The coordination spheres of all CPs show distorted octahedral geometries. CP **3** was mainly tested as heterogenous catalyst for peroxidative oxidation of benzyl alcohol and its derivatives (4-chloro, 4-bromo, 4-methyl, 4-metoxy and 4-nitro benzyl alcohol). From the results, the highest aldehyde formation was obtained from the oxidation of benzyl alcohol with overall yield as 100%. In addition, catalytic reactions exhibited high selectivity towards aldehyde and no over-oxidation product (carboxylic acid) was observed.

Keywords Hexacyanochromate(III) · Hexacyanoferrate(III) · Hexacyanocobaltate(III) · 3-(Aminomethyl)pyridine complex · Coordination polymer · 2D complex · 3D complex · Catalyst

1 Introduction

Recently, the design and synthesis of coordination polymers (CPs) has received great attention because CPs have potential applications in many fields such as luminescence [1], electronic devices [2], magnetism [3–5] and catalysis [6, 7]. In general, CPs are formed by metal centres and organic ligands through coordination bonds, where metals act as binders and organic ligands act as chains. Although the design and synthesis of CPs have made significant advances, their predictable and controlled synthesis with desired structures and properties is still a major challenge. Supramolecular interactions refer to non-covalent interactions between molecules that are weaker than chemical bonds but play a crucial role in shaping the structure and properties of complex molecular assemblies. These interactions include hydrogen bonding, van der Waals forces, hydrophobic interactions, π–π stacking, and electrostatic interactions. They are essential in biological processes, self-assembly of materials, and various other fields of science. Like this systems with supramolecular properties have one-dimensional (1D, zigzag or straight chain), two-dimensional (2D) and three-dimensional skeletal (3D, layered) structure. Hydrogen bonds, a supramolecular interaction, perform a structural role because they permit the correct orientation of magnetic orbitals on adjacent paramagnetic centers [8]. For the formation of novel complexes, non-covalent interactions such as hydrogen bonds [9], π-π bonds [10], C–H···π [11] and anion···π [12] interactions are crucial. D–H···M (D = C,

✉ Güneş Süheyla Kürkçüoğlu
gkurkcuo@ogu.edu.tr

[1] Department of Physics, Faculty of Science, Eskişehir Osmangazi University, 26040 Eskisehir, Turkey

[2] Department of Chemistry, Faculty of Science, Eskişehir Technical University, 26555 Eskisehir, Turkey

[3] Department of Occupat Health & Safety, School of Health, Sinop University, 57000 Sinop, Turkey

[4] Department of Chemistry, Faculty of Science, Eskişehir Osmangazi University, 26040 Eskisehir, Turkey

N, or O) interactions can also occur between a metal center and a hydrogen atom [13].

Cyanide ligands allow easy design of organic–inorganic polynuclear assemblies and cyanide complexes, which have a special place in CPs, are quite remarkable complexes both in terms of structure and application. Such complexes were among the first coordination compounds synthesized and studied [14–17]. It is also a versatile and important group of molecule-based functional materials [18]. In addition to the many uses of CPs, their catalytic activities are often the subject of research [19, 20]. Among these research areas, catalytic alcohol oxidation reactions have an important place [21]. Cyanide-bridged CPs have been investigated for next-generation chemical designs due to their magnetic, optical, electrical, catalytic and biological properties [5, 22–27]. Besides that organic ligands can be used to enable the formation of 1D, 2D and 3D dimensional layers as well as polynuclear structures, chains and layers [28]. Various examples of hexacyanometallate(III) complexes have been reported previously [29–34]. In the literature, it was seen that various complexes were obtained by using both 3ampy ligand and hexacyanometallate(III) ions [35–42].

Catalytic alcohol oxidation is one of the biggest challenges in synthetic organic chemistry because it is necessary to obtain the corresponding aldehydes and ketones [43, 44]. Researchers have long sought highly selective metal catalysts to carry out these catalytic reactions. Products obtained from the oxidation of alcohols, mainly used in chemical industry as starting or intermediate compounds to synthesize much more complex chemicals. Although there are various oxidant alternatives in the oxidation of alcohols, most of them conducted with using harmful heavy metal-containing oxidants such as CrO_3, PCC, $KMnO_4$, in which the oxidant is used as stoichiometric. Instead of these harmful oxidants, environment-friendly alternatives that do not contain heavy metals (such as; t-BuOOH, H_2O_2 vb) are tried to be used in chemical transformations.

During this study, three new CPs with 3ampy ligand and hexacyanometalate(III) ions ($[M(CN)_6]^{3-}$, M = Cr, Fe or Co), $[Cd_3(\mu\text{-}3ampy)_4(H_2O)_4Cr_2(\mu\text{-}CN)_8(CN)_4]_n$ (**1**), $[Cd_3(\mu\text{-}3ampy)_2(H_2O)_2Fe_2(\mu\text{-}CN)_5(CN)_7]_n$ (**2**) and $[Cd_3(\mu\text{-}3ampy)_4(H_2O)_4Co_2(\mu\text{-}CN)_8(CN)_4]_n$ (**3**), (3ampy = 3-(aminomethyl)pyridine) were synthesized and characterized by vibration (FT-IR and Raman) spectroscopy, crystallographic (SC-XRD and PXRD), elemental and thermal analyses. In addition, the catalytic performance of CP **3** was investigated in the oxidation of benzyl alcohol and derivatives with *tert*-Butyl hydroperoxide (TBHP) in several organic solvents.

2 Experimental

2.1 Materials and Physical Measurements

Cadmium(II) acetate dihydrate ($Cd(CH_3COO)_2{\cdot}2H_2O$, Acros, 99%), Potassium hexacyanochromate(III) ($K_3[Cr(CN)_6]$, Sigma-Aldrich, 99.99%), Potassium hexacyanoferrate(III) ($K_3[Fe(CN)_6]$, Merck, 99%), Potassium hexacyanocobaltate(III) ($K_3[Co(CN)_6]$, Acros, 95%), and 3-(aminomethyl)pyridine ($C_6H_8N_2$, Alfa Aesar, 98%) and ammonia solution (NH_4OH, Merck, 25%) were purchased from commercial sources and were used as received.

Elemental analysis results were taken on LECO CHNS-932 analyzer for C, H and N. FT-IR spectra were recorded with a Perkin Elmer 100 FT-IR spectrometer (calibrated using polystyrene and CO_2 bands) with ATR (Atenuated Total Reflection) at 4000–250 cm^{-1} (4 cm^{-1} resolution). Raman spectra were recorded in the Bruker Senterra Dispersive Raman instrument at the range of 4000–250 cm^{-1} using 785 nm laser excitation. Powder X-ray diffraction (PXRD) patterns were obtained from a PANALYTICAL EMPYREAN X-ray diffraction instrument operating at 40 kV and 30 mA with Cu-Kα radiation (λ = 1.5406 nm). The Perkin Elmer Diamond TG/DTA Thermal Analyzer was used at a heating rate of 10 °C/min in a temperature range of 30–1000 °C in a static atmosphere to record the TG, DTG and DTA curves.

2.2 X-Ray Diffraction Analysis

For all structures, data collection which was performed on a Bruker diffractometer equipped with a graphite-monochromatic Mo-Kα radiation at 296 K. We used these procedures for our analyses: solved by direct methods; SHELXS-2013 [45]; refined by full-matrix least-squares methods; SHELXL-2013 [46]; data collection: Bruker APEX2 [47]; molecular graphics: MERCURY [48]; solution: WinGX [49]. Crystal data, data collection and refinement details for **1–3** are summarized in Tables 1, 2, and 3. Some bad outlier reflections (1–21, 001, 011 for **1**, 001 for **2** and 011 for **3**) were omitted from the data set for **1–3**. The positions of the H atoms of the $–OH_2$ groups were found in difference Fourier maps and refined isotropically. All other H atoms were located in difference maps and then treated as riding atoms in geometrically idealized positions, with C–H distances of 0.93–0.97 Å and $U_{iso}(H) = 1.2U_{eq}(C)$ and N–H distances of 0.97 Å and $U_{iso}(H) = 1.2U_{eq}(N)$.

Table 1 Crystal data and structure refinement parameters for **1**–**3***

Crystal data	**1**	**2**	**3**
Empirical formula	$C_{36}H_{40}Cd_3Cr_2N_{20}O_4$	$C_{36}H_{40}Cd_3Fe_2N_{20}O_4$	$C_{36}H_{40}Cd_3Co_2N_{20}O_4$
Formula weight	1258.08	1265.78	1271.94
Crystal system	Triclinic	Monoclinic	Triclinic
Space group	*P*-1	*C*2/m	*P*-1
a (Å)	8.6913(12)	15.3330(11)	8.5178(6)
b (Å)	9.6361(15)	14.5177(11)	9.4100(6)
c (Å)	15.066(2)	10.6762(8)	14.903(1)
α (°)	92.182(5)	90.00	90.732(2)
β (°)	94.337(4)	93.085(4)	94.577(3)
γ (°)	106.423(5)	90.00	106.469(2)
V (Å^3)	1204.5(3)	2373.1(3)	1141.07(13)
Z	1	2	1
Temperature (K)	296	296	296
D_c (g cm^{-3})	1.734	1.771	1.851
μ (mm^{-1})	1.80	1.98	2.15
θ range (°)	2.5–26.3	2.7–27.8	2.6–27.6
Measured refls	34,289	38,400	42,714
Independent refls	5975	3077	5700
R_{int}	0.050	0.053	0.083
S	1.03	1.10	1.06
R1/wR2	0.031/0.063	0.030/0.053	0.045/0.075
$\Delta\rho_{max}/\Delta\rho_{min}$ (eÅ^{-3})	0.74/− 0.66	0.81/− 0.63	0.98/− 0.95

*Crystallographic data for the structural analyses have been deposited with the Cambridge Crystallographic Data Centre, CCDC No 2130451 for 1, 2130452 for 2, 2130453 for 3

Table 2 Selected bond distances for **1**–**3** (Å,°)

1					
Cd1-N3	2.333(2)	Cd1-N7^{i}	2.392(2)	Cd1-N2	2.397(2)
Cd2-O2	2.304(2)	Cd2-N4	2.310(2)	Cd2-N5	2.368(3)
Cd2-O1	2.382(2)	Cd2-N1^{ii}	2.389(2)	Cd2-N10^{iii}	2.400(3)
Cr1-C13	2.094(3)	Cr1-C14	2.076(3)	Cr1-C15	2.075(3)
Cr1-C16	2.051(3)	Cr1-C17	2.074(3)	Cr1-C18	2.089(3)
2					
Cd1-N8	2.339(3)	Cd1-O1	2.353(3)	Cd1-N1	2.382(2)
Cd1-N4^{i}	2.396(3)	Cd2-N3	2.359(3)	Cd2-N2	2.384(2)
Fe1-C7	1.943(4)	Fe1-C8	1.945(4)	Fe1-C9	1.956(4)
Fe2-C12	1.930(4)	Fe2-C10	1.943(4)	Fe2-C11	1.967(4)
3					
Cd1-O1	2.284(4)	Cd1-N1	2.293(4)	Cd1-N3	2.392(4)
Cd1-N5	2.400(4)	Cd1-O2	2.407(3)	Cd1-N9^{i}	2.414(4)
Cd2-N2	2.320(3)	Cd2-N4^{i}	2.399(4)	Cd2-N6^{ii}	2.401(4)
Co1-C13	1.909(5)	Co1-C14	1.908(5)	Co1-C15	1.904(5)
Co1-C16	1.893(5)	Co1-C17	1.895(5)	Co1-C18	1.908(5)

Symmetry codes: (i) x − 1, y − 1, z; (ii) − x, − y, − z + 1; (iii) x − 1, y, z for **1**; (i) − x + 1/2, − y + 1/2, − z + 1 for **2**; (i) x − 1, y, z; (ii) x − 1, y − 1, z for **3**

2.3 Syntheses of the CPs

1 mmol cadmium(II) acetate dihydrate (0.266 g) dissolved in 20 mL water was added dropwise upon stirring to solution of 1 mmol $K_3[M(CN)_6]$ {$K_3[Cr(CN)_6] = 0.325$ g, $K_3[Fe(CN)_6] = 0.329$ g and $K_3[Co(CN)_6] = 0.332$ g} in 15 mL water and 5 mL ammonium hydroxide solution. After stirring for 15 min, 4 mmol 3ampy (0.432 g) dissolved in 10 mL ethanol and 10 mL water was added to these stirring solutions separately. These solutions were stirred at 50 °C for 5 h in the magnetic stirrer. Yellow crystals of $[Cd_3(\mu\text{-}3ampy)_4(H_2O)_4Cr_2(\mu\text{-}CN)_8(CN)_4]_n$ (**1**) were acquired in 35% yield (based on $Cd(CH_3COO)_2{\cdot}2H_2O$) Analyses calculated for $C_{36}H_{40}Cd_3Cr_2N_{20}O_4$ (**1**) (MW = 1258.08 gmol^{-1}): C 34.30, H 3.59, N 24.10%; found C 34.37, H 3.20, N 23.27%. Yellow crystals of $[Cd_3(\mu\text{-}3ampy)_2(H_2O)_2Fe_2(\mu\text{-}CN)_5(CN)_7]_n$ were acquired in 51% yield (based on $Cd(CH_3COO)_2{\cdot}2H_2O$) Analyses calculated for $C_{36}H_{40}Cd_3Fe_2N_{20}O_4$ (**2**) (MW = 1265.78 gmol^{-1}): C 34.00, H 3.56, N 25.10%; found C 34.16, H 3.19, N 25.10%. White crystals of $[Cd_3(\mu\text{-}3ampy)_2(H_2O)_2Fe_2(\mu\text{-}CN)_5(CN)_7]_n$ were acquired in 52% yield (based on $Cd(CH_3COO)_2{\cdot}2H_2O$) Analyses calculated for $C_{36}H_{40}Cd_3Co_2N_{20}O_4$ (**3**) (MW = 1271.94

Table 3 Hydrogen-bond parameters for **1**–**3** (Å,°)

D–H···A	D–H	H···A	D···A	D–H···A
1				
N2–H2C···N8^{viii}	0.97	2.22	3.058(4)	144
N2–H2D···N6^{iv}	0.97	2.48	3.255(4)	137
N3–H3A···N8^{viii}	0.97	2.19	3.021(4)	143
N3–H3B···N6^{v}	0.97	2.17	3.127(4)	168
O1–H1A···N10^{ix}	0.85	2.140	2.951(3)	160
O1–H1B···N9^{ii}	0.84	1.900	2.728(4)	171
O2–H2B···O1^{x}	0.87	2.34	3.046(3)	138
O2–H2A···N5^{ix}	0.86	2.62	3.446(4)	162
2				
C1–H1···N3^{ii}	0.93	2.63	3.402(4)	141
N2–H2A···N6	0.97	2.27	3.060(4)	138
N2–H2B···N7^{viii}	0.97	2.44	3.378(4)	161
O1–H1B···N8^{ix}	0.87	2.43	3.244(4)	156
O1–H1A···N5^{x}	0.88	2.280	3.150(4)	170
3				
O1–H1A···N5^{viii}	0.85(2)	2.54(2)	3.382(6)	172(6)
O1–H1B···O2^{ix}	0.85(2)	2.30(4)	3.008(6)	140(5)
O2–H2A···N7^{v}	0.83(2)	1.92(2)	2.743(5)	176(6)
O2–H2B···N9^{viii}	0.83(2)	2.15(2)	2.944(5)	161(4)
N2–H2C···N8^{x}	0.97	2.19	3.019(6)	143
N2–H2D···N10^{i}	0.97	2.22	3.172(6)	167
N4–H4A···N10	0.97	2.56	3.319(6)	136
N4–H4B···N8^{v}	0.97	2.24	3.077(6)	144

Symmetry codes: (ii) x − 1, y − 1, z; (iv) − x, − y, − z + 1; (v) x − 1, y, z; (viii) − x + 1, − y + 1, − z + 1; (ix) − x + 1, − y + 1, − z + 2; (x) − x, − y + 1, − z + 2 for **1**, (ii) − x + 1/2, − y + 1/2, − z + 1; (viii) x − 1/2, y + 1/2, z; (ix) − x + 1, − y, − z; (x) x, y − 1, z − 1 for **2**, (i) x − 1, y, z; (v) x − 1, y − 1, z; (viii) − x + 1, − y + 1, − z + 1; (ix) − x, − y + 1, − z + 1; (x) − x + 1, − y + 1, − z for **3**

gmol^{-1}): C 33.40, H 3.53, N 23.90%; found C 33.99, H 3.17, N 23.02%.

2.4 Peroxidative Oxidation

The peroxidative oxidation reactions were conducted as follows: calculated amounts of benzylic alcohol, catalyst and 70% aqueous solution of TBHP were added in a 4 mL of organic solvent and the final solution kept at required temperature. To reach up to 15°–20° above than the boiling points of solvents catalytic reactions were carried out with using high pressure reaction tubes**.** Reaction samples were taken at certain time intervals (2 h, 4 h, 6 h and 24 h), treated with triphenylphosphine (PPh_3) to reduce the excess peroxide [50] and analyzed on gas chromatography device with an HP-5 quartz capillary column (30 m × 0.32 mm × 0.25 µm) with a flame ionization detector (FID) to observe the substrate/product(s) percentage distributions. The catalytic results are given in Tables 4 and 5.

3 Results and Discussion

3.1 Structural Analysis of the CPs

The single crystal X-ray study shows that the heterometallic CPs **1** and **3** are 2D CPs while the heterometallic CP **2** shows a 3D polymeric coordination arrangement. The crystallographic analyses show that CPs **1** and **3** appear very similar. **1** and **3** have *P*-1 space group, while **2** is *C*2/m. The asymmetric unit of **1** and **3** consists of two Cd(II) ions, one M ion [M = Cr(III) in **1** and Co(III) in **3**], six cyanide ligands, two 3ampy ligands and two coordinated water molecules (Fig. 1a, c). In CP **2**, the asymmetric unit consists of two Cd(II) ions, two Fe(III) ions, six cyanide ligands, one 3ampy ligand and one coordinated water molecule. In CPs **1–3**, the Cd(II) ions are of two coordination sphere. In the first of these coordination, each Cd(II) ion [Cd = Cd1 in **1**, Cd2 in **2** and Cd2 in **3**] is coordinated by four nitrogen atoms from 3ampy ligands and two nitrogen atoms from cyanide ligands (Table 2). In the second coordination, each Cd(II) ion [Cd = Cd2 in **1**, Cd1 in **2** and Cd1 in **3**] is coordinated by two nitrogen atoms from 3ampy ligands, two nitrogen atoms from cyanide ligands and two oxygen atoms from water molecules. Each M ion [M = Cr(III) in **1**, Fe(III) in **2** and Co(III) in **3**] is coordinated by six carbon atoms from cyanide ligands. In CPs **1–3**, the coordination spheres of all metal ions show distorted octahedral coordination geometry. The Cd(II) ions are bridged by 3ampy ligands to generate [Cd_3(3ampy)$_3$] units, with the Cd(II)···Cd(II) separations are 8.225(3) and 8.381(3) Å in **1**, 8.775(3) Å in **2** and 8.201(4) and 8.301(4) Å in **3**. Similarly, the combination of ligands and ions produce [$Cd_3M(CN)_2$(3ampy)$_2$] [M = Cr(III) in **1**, Fe(III) in **2** and Co(III) in **3**] units, with the Cd(II)···M separations are 5.286(3) and 5.481(3) Å in **1**, 4.931(3) Å in **2** and 5.090(4) and 5.336(4) Å in **3**. The combination of these units produces 3D CP in **2** and 2D CPs in **1** and **3** (Fig. 2a, c). In **1** and **3**, adjacent 2D supramolecular networks are joined by O–H···N, O–H···O and N–H···N hydrogen bonds, generating 3D supramolecular network (Table 3).

3.2 Powder X-Ray Diffraction (PXRD) Analyses

Powder X-ray diffraction (PXRD) patterns of the CPs were used to check the phase purity of CPs **1–3** (Fig. S1). Simulated PXRD patterns were obtained using Mercury

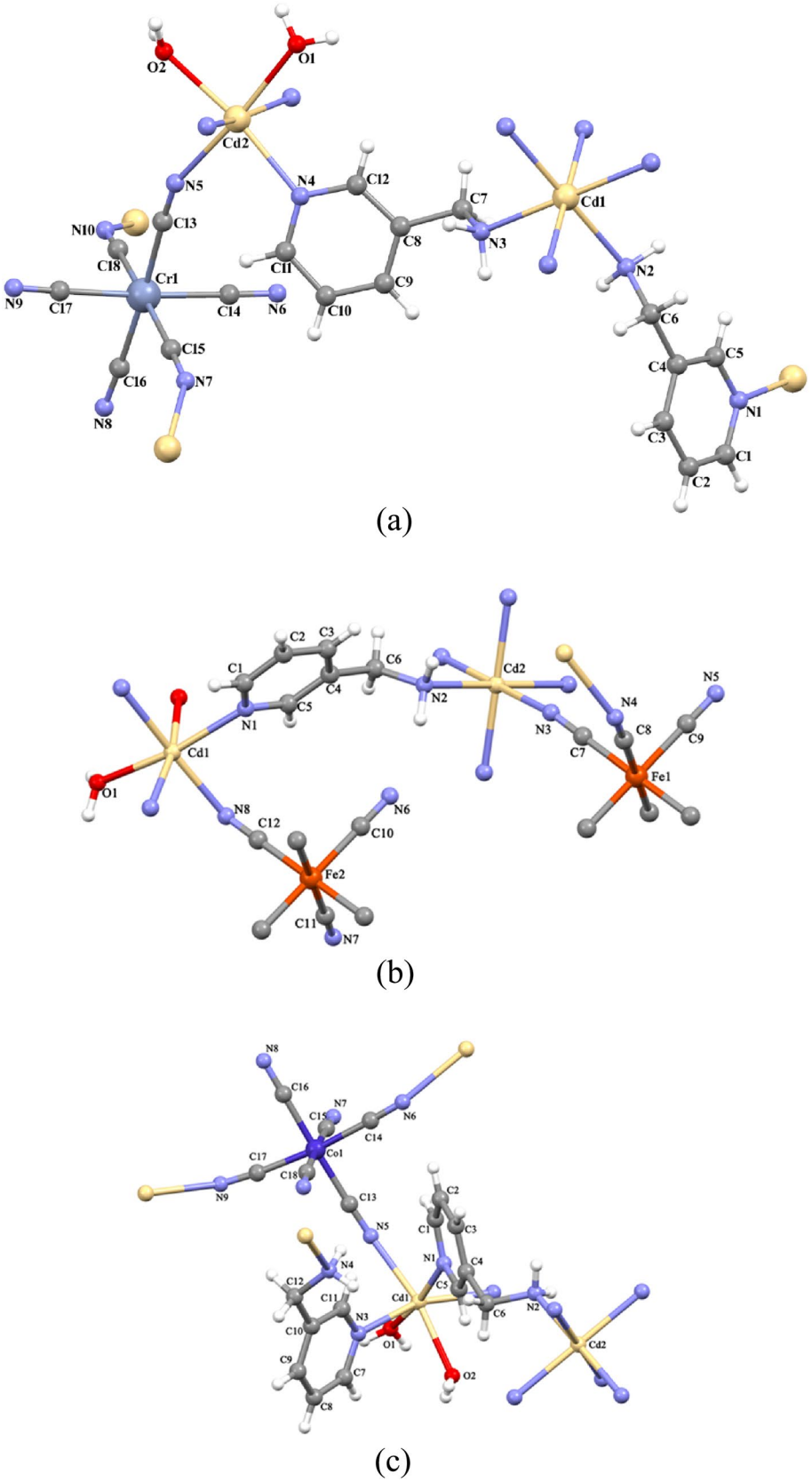

Fig. 1 The molecular structures of **a 1**, **b 2** and **c 3** showing the atom numbering schemes

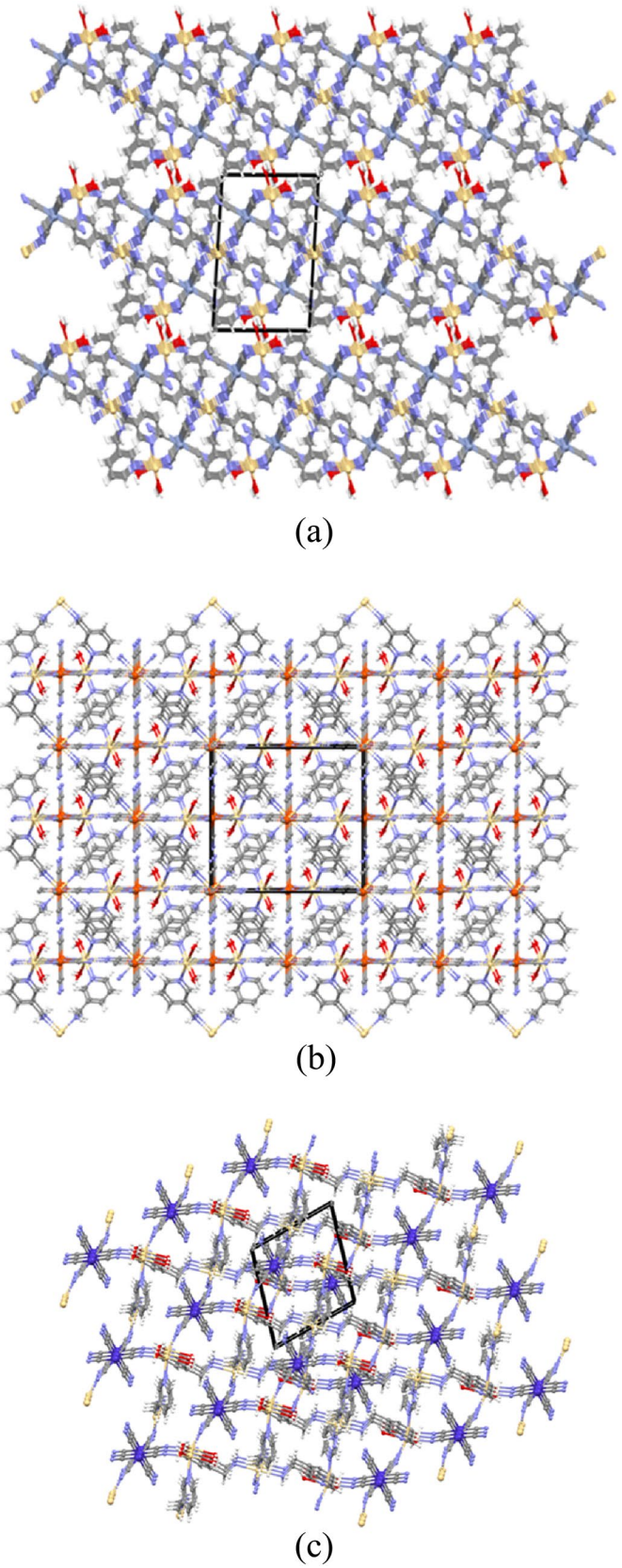

Fig. 2 An infinite 3D network in **a 1**, **b 2** and **c 3**

CSD software based on single crystal data. Comparing the simulated and experimental PXRD models, it was seen that there was a good agreement indicating that the crystal products were in pure phase.

3.3 Vibrational Analyses

Vibrational (FT-IR and Raman) spectra of the CPs are shown in Figs. S2 and S3. Symmetrical and asymmetrical ν(OH) stretching vibrations of the aqua ligands in the CPs were observed in the region of 3450–3350 cm^{-1}, and δ(OH) bending vibrations were observed in the range of 1630–1620 cm^{-1} wavenumbers. According to this, asymmetric and symmetrical ν(OH) stretching vibration wavenumbers were found to be 3339 cm^{-1} for **1**, 3442 cm^{-1} for **2**, and 3450 cm^{-1} for **3**. In addition, δ(OH) bending vibrations have wavenumber values of 1628 cm^{-1}, 1630 cm^{-1} and 1628 cm^{-1} in the CPs, respectively.

In literature, stretching vibrations ν(NH) resulting from -NH_2 vibrations are found in the wavenumber range of 3400–3100 cm^{-1} [51]. Asymmetric and symmetrical ν(NH) stretching vibration wavenumbers were observed in the range of 3352–3274 cm^{-1} of 3ampy molecules in the FT-IR spectra. It was determined that these vibrations in the CPs shifted to 6–7 cm^{-1} higher wavenumbers compared to 3ampy ligand [52]. However, δ(NH_2) bending vibrations were observed at 1583 cm^{-1} for **1** and **2** and, at 1589 cm^{-1} for **3**. The positions of the ν(CN) stretching bands in the FT-IR spectra of the complexes containing cyanide ligands are a significant instrument for determining the number and type (terminal or bridging) of cyanide groups in the complexes. The (CN) stretching frequency of a terminal cyanide ligand ranges from 2000–2100 cm^{-1}, whereas the range 2100–2200 cm^{-1} is characteristic of a cyanide ligand that functions as a bridge and a terminal cyanide ligand involved in hydrogen bond interactions [53–56]. CPs **1–3** include two cyanide stretching bands are observed in the FT-IR spectra at 2134 cm^{-1} and 2122 cm^{-1} for **1**, 2125 cm^{-1} and 2096 cm^{-1} for **2** and 2121 cm^{-1} and 2118 cm^{-1} for **3**.

The FT-IR and Raman spectral data of the CPs were compared with the crystallographic data and the results appear to be consistent with each other. Terminal cyanide frequencies $\nu(CN)_t$ in cyanide complexes usually appear at frequencies lower than that of the bridging cyanide frequencies $\nu(CN)_b$ [53].

3.4 Thermal Analyses

Thermal analyses of the **1–3** were performed in a static air atmosphere with a heating rate of 10 °C per minute in the range of 30 to 1000 °C and the TG, DTA and DTG curves are shown in Fig. S4. The thermal decomposition of **1–3** proceeds in three stages. In the first stage, the **1–3** lose aqua ligands in the temperature range 67–220 °C [found (calcd., %) = 7.64 (7.15)] for **1;** 30–130 °C [found (calcd., %) = 7.12 (6.59)] for **2** and 30–200 °C [found (calcd., %) = 7.52 (7.01)] for **3**. The second stage is related to release of 3ampy ligands in the temperature range 220–333 °C [found (calcd.)(%) = 20.02 (19.57)] for **1**; 130–407 °C [found (calcd., %) = 21.13 (21.25)] for **2** and 200–312 °C [found (calcd., %) = 19.14 (19.21)] for **3.** In the last stage between 423 and 815 °C temperature range for **1**; between 407 and 499 °C temperature range for **2** and between 312 and 446 °C temperature range for **3**, strong exothermic peak ($DTA_{max.}$ = 416 °C for **1**; 473 °C for **2** and 397 °C for **3**) is associated with the burning of the remaining cyanide ligands and leading finally to the CdO and Cr_2O_3 for **1;** CdO and Fe_2O_3 for **2** and CdO and Co_2O_3 for **3**. The final solid products of thermal decompositions were identified by FT-IR spectroscopy (found (calcd.)(%) = 55.45 (56.31) for **1**; 58.43 (58.26) for **2** and found: 60.02 (59.29) for **3**.

Table 4 Catalytic oxidation results of benzyl alcohol to benzaldehyde with using **3**

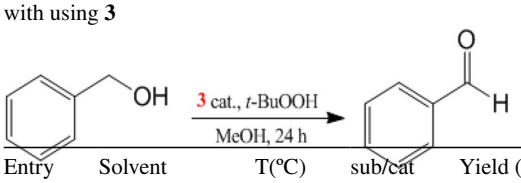

Entry	Solvent	T(°C)	sub/cat	Yield (%)	TON
1	EtOH	80	200	5.9	12
2	CH_3CN	80	200	27.2	54
3	MeOH	80	200	31.4	62
4	THF	80	200	0.6	2
5	DMF	80	200	4.2	8
6	$CHCl_3$	80	200	6.2	12
7	1,4-Dioxane	80	200	21.3	42
8	Toluene	80	200	29.1	58
9	MeOH	80	100	**85.4**	**85**
10	MeOH	60	100	28.6	29
11	MeOH	40	100	24.3	24
12	MeOH	20	100	19.8	20
13[a]	MeOH	80	—	Trace	–
14[b]	MeOH	80	100	25.1	25
15[c]	MeOH	80	100	32.4	32

Conditions with the highest conversion are shown in bold.

Yields and TONs determined by GC analysis (upon treatment with PPh_3)

Reaction conditions: $n_{Benzyl\ Alcohol}$ = 0.1 mmol, $M_{Benzyl\ Alcohol}$ = 0.02 M, $V_{solv.}$ = 4 mL, $V_{t\text{-}BuOOH}$ = 1 mL, $M_{t\text{-}BuOOH}$ = 1.44 M, *t* = 6 h; [a]Without catalyst, [b]With **1**, [c]With **2**

3.5 Catalytic Studies

In general, benzyl alcohol is selected as a model substrate in the catalytic oxidation of primary benzylic alcohols owing to its reactivity [57]. It is clearly known that the solvent effect is an important parameter in catalytic reactions [27]. For this reason, to examine the effect of solvent

Table 5 Substrate effect on oxidation reaction by catalyst **3**

Entry	Primary alcohol	Product yield (%)	TON
1	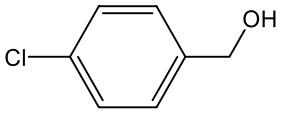	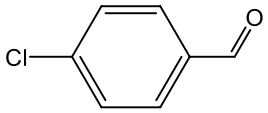 18.4 (6h) 41.8 (24h)	42
2	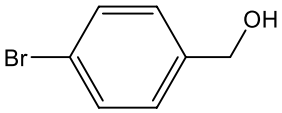	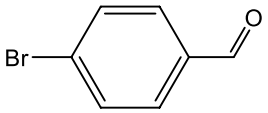 21.7 (6h) 55.6 (24h)	56
3	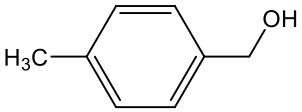	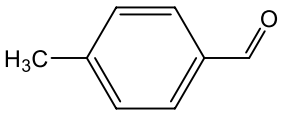 17.1 (6h) 27.1 (24h)	27
4	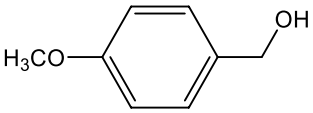	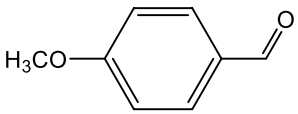 20.8 (6h) 42.1 (24h)	42
5	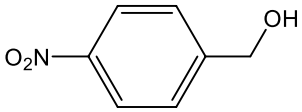	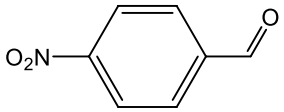 22.5 (6h) 39.2 (24h)	39

Reaction conditions: $n_{Alcohol} = 0.1$ mmol, $M_{Alcohol} = 0.02$ M, $V_{solv.} = 4$ mL, $V_{t\text{-}BuOOH.} = 1$ mL, $M_{t\text{-}BuOOH} = 1.44$ M, s/c = 100, T = 80 ºC, $t = 6$ h. Yields and TONs determined by GC analysis (upon treatment with PPh_3)

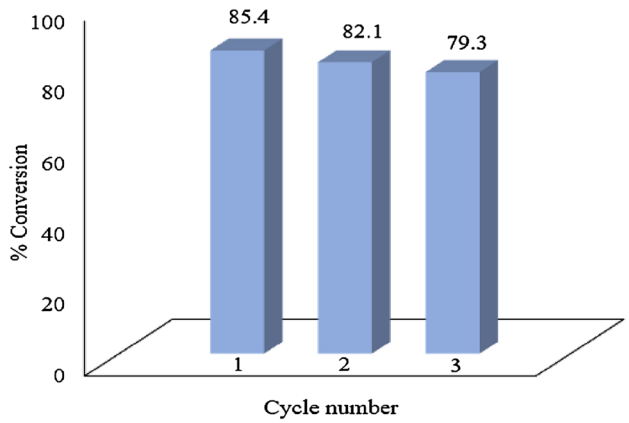

Fig. 3 Reusability tests for benzyl alcohol oxidation with CP **3**

on catalytic activity, eight different organic solvents having various polarities, including ethyl alcohol (EtOH), acetonitrile (CH_3CN), methyl alcohol (MeOH), tehrahydrofuran (THF), *N,N'*-dimethylformamide (DMF), chloroform ($CHCl_3$), 1,4-dioxane and toluene were selected. We would like to point out in particular that, no acid formation was observed in any solvent medium. The results proved that, synthesized catalyst serves selectively. As seen in Table 4, as a result of solvent nature, aldehyde formation percentages veried between 0.6–31.4% after 6-h reaction time at 80 °C (Entries 1–8). The solvents in which the product (aldehyde) formations remained below 10% were determined as THF (0.6%), DMF (4.2%), EtOH (5.9%) and $CHCl_3$ (6.2%), respectively (Entries 1, 4–6). The highest product formation was observed when MeOH was used with the conversion value of 31.4% under the same

Table 6 Comparison of some catalytic MOF systems for the oxidation of benzyl alcohol

Entry	Catalyst	Cat. (%)	Additive	Base	Oxidant	TON	References
1	Cu-FMOF	10	TEMPO	DMAP	Open air	10	[62]
2	Cu-MOF-74	5	TEMPO	Na_2CO_3	Molecular O_2	18	[63]
3	**3**	1	––	––	TBHP	85	This work

conditions (Entry 3). To take the entire solvent results into account, the reactivity order of conversion results was detected as CH_3OH > Toluene > CH_3CN > 1,4-Dioxane > $CHCl_3$ > EtOH > DMF > THF. As a result, MeOH is considered to be the most suitable solvent.

Substrate/catalyst (s/c) ratio is an important issue in catalysis [58]. To increase the benzaldehyde yield, s/c ratio decreased from 200 to 100 while the other parameters kept constant. It was observed that, highest product formation (85.4%) was detected after 6 h (Entry 9). After that, to examine the effect of temperature on the reaction, 60, 40 and 20 °C were chosen. As expected, the conversion of benzyl alcohol decreases from 28.6 to 19.8% with decreasing reaction temperature, under the same conditions (Entries 10–12). A blank experiment was also conducted (Entry 13). In addition, the other two catalysts (catalysts **1** and **2**) were tested in the conditions where the highest activity was achieved, but it was determined that they were not as effective as catalyst **3** (25.1% for catalyst **1** and 32.4% for catalyst **2**).

The effect of the chemical structure of the substrate on the catalytic oxidation of alcohols is an important research step. Numerous research examples can be given in the literature on this subject [59–61]. To investigate the substrate effect, reactions were carried out under the optimized conditions (s/c = 100, 80 °C and 6-h reaction time). When the results were examined, it was found that there was no significant difference in the conversion percentages, despite carrying electron withdrawing and donating groups on the substrates (Table 5). Similar aldehyde formations were detected (around 20%) for all substrates after 6-h reaction time (Entries 1–5). To increase the product formations, reaction times extended to 24 h under the same conditions. By using 4-bromobenzyl alcohol, 55.6% aldehyde formation was observed as the highest obtained product yield (Entry 2).

Catalytic alcohol oxidation studies are frequently encountered in the literature [62, 63]. However, it is difficult to find similar studies in which heteronuclear CPs are used as catalysts. For this reason, we will give examples from heterogeneous catalysis studies with CPs in which benzyl alcohol is used as a model substrate. Compared to some MOF catalyst systems, the presented system has better activity without the use of any additives (TEMPO, base, etc.). In the presented study, TON values are much higher than Cu-MOF-74 (TON = 18) and $([Cu_2(1,2\text{-BDC})_2(Fbtx)_2]0.3H_2O)_n$ (TON = 10) MOF systems. In addition, the amount of catalysts higher than the presented system as 5 and 10% of alcohol, respectively.

3.6 Reusability Tests

One advantage of heterogeneous catalytic systems is that they can be reused. The catalyst was reused 3 times under conditions where the highest efficiency was achieved with the model substrate (Fig. 3). After each cycle, the catalyst was filtered, washed and ready for reuse. As a result of the experiments, no significant change was detected in the catalyst activity. These results show us that there is no deterioration in the catalyst structure (Table 6).

4 Conclusions

In this study, three new heteronuclear metal-cyanide CPs were synthesized under similar conditions using hexacyanometallates(III) (Cr, Fe and Co) ions and 3ampy ligand. In CPs **1**–**3**, the coordination spheres of all ions show distorted octahedral coordination geometry. Heterometallic CPs **1** and **3** have 2D CP while heterometallic CP **2** has 3D CP. In **1** and **3**, adjacent 2D supramolecular networks are joined by O–H···N, O–H···O and N–H···N hydrogen bonds, generating 3D supramolecular network. **1**–**3** show extremely interesting architectures composed of 3ampy and cyanide ligands. Furthermore, the catalytic activities for the peroxidative oxidation of benzylic alcohols in **3** was also investigated. Basically, **3** has been used as a heterogeneous catalyst for the peroxidative oxidation of some benzyl alcohol and its derivatives. The highest aldehyde formation from the results was obtained from the oxidation of benzyl alcohol, in general, 100% yield.

Supplementary Information The online version contains supplementary material available at https://doi.org/10.1007/s10904-023-02861-z.

Acknowledgements The authors acknowledge Scientific and Technological Research Application and Research Center, Sinop University, Turkey, for the use of the Bruker D8 QUEST diffractometer.

Author Contributions All authors share equally in writing the main manuscript, preparing the figures and reviewed the manuscript.

Funding This work has been financially supported by Eskişehir Osmangazi University, Scientific research Unit [Grant No: 2022-2561].

Declarations

Conflict of interest The authors declare that they have no confict of interest.

References

1. Y. Zhang, S. Yuan, G. Day, X. Wang, X. Yang, H.C. Zhou, Coord. Chem. Rev. **354**, 28–45 (2018)
2. L. Zhang, H. Liu, W. Shi, P. Cheng, Coord. Chem. Rev. **388**, 293–309 (2019)
3. J.H. Jia, Q.W. Li, Y.C. Chen, J.L. Liu, M.L. Tong, Coord. Chem. Rev. **378**, 365–381 (2019)
4. R. Bikas, H. Hosseini-Monfared, V. Vasylyeva, J. Sanchiz, J. Alonso, J.M. Barandiaran, Dalton Trans. **43**(31), 11925–11935 (2014)
5. N. Rad-Yousefnia, B. Shaabani, M. Korabik, M. Weselski, M. Zahedi, U. Englert, Dalton Trans. **48**(30), 11421–11432 (2019)
6. L.L. Qian, Z.X. Wang, H.X. Tian, M. Li, B.L. Li, H.Y. Li, Acta Crystallogr. Sect. C **75**(8), 1053–1059 (2019)
7. T. Mwanza, G.S. Kürkçüoğlu, H. Ünver, O. Şahin, O.Z. Yeşilel, J. Solid State Chem. **314**, 123344 (2022)
8. C. Desplanches, E. Ruiz, A. Rodríguez-Fortea, S. Alvarez, J. Am. Chem. Soc. **124**(18), 5197–5205 (2002)
9. T. Steiner, Angew. Chem. Int. Ed. **41**(1), 48–76 (2002)
10. G.S. Kürkçüoğlu, E. Sayın, O. Şahin, J. Mol. Struct. **1101**, 82–90 (2015)
11. K. Gör, G.S. Kürkçüoğlu, O.Z. Yeşilel, O. Büyükgüngör, Inorg. Chim. Acta **414**, 15–20 (2014)
12. H.T. Chifotides, K.R. Dunbar, Acc. Chem. Res. **46**(4), 894–906 (2013)
13. S. González-Montiel, D. Martínez-Otero, N. Andrade-López, J.G. Alvarado-Rodríguez, M. Carmona-Pichardo, J. Cruz-Borbolla, T. Pandiyan, L.W. Pineda, Polyhedron **87**, 181–193 (2015)
14. A. M. Golub, H. Kohler, Chemie der Pseudohalogenide, VEB 224 Deutscher Verlag der Wissenschaften, Berlin (1979)
15. K. Hofmann, F. Küspert, Z. Anorg. Allg. Chem. **15**(1), 204–207 (1897)
16. A. Ludi, Chem. Unserer Zeit. **22**(4), 123–127 (1988)
17. A.G. Sharpe, *The Chemistry of the Cyano Complexes of the Transition Metals* (Academic Press, London, 1976), p.302
18. M. Heczko, E. Suminska, D. Pinkowicz, B. Nowicka, Inorg. Chem. **61**(35), 13817–13828 (2022)
19. A. Dhakshinamoorthy, Z. Li, H. Garcia, Catalysis and photocatalysis by metal organic frameworks. Chem. Soc. Rev. **47**(22), 8134–8172 (2018)
20. Y.S. Kang, Y. Lu, K. Chen, Y. Zhao, P. Wang, W.Y. Sun, Coord. Chem. Rev. **378**, 262–280 (2019)
21. L. Asgharnejad, A. Abbasi, M. Najafi, J. Janczak, J. Solid State Chem. **277**, 187–194 (2019)
22. M. Liu, J. Hu, Y. Wang, Polyhedron **149**, 79–83 (2018)
23. J. Černák, M. Orendáč, I. Potočňák, J. Chomič, A. Orendáčová, J. Skoršepa, F. Alexander, Coord. Chem. Rev. **224**(1–2), 51–66 (2002)
24. C. Janiak, Dalton Trans. **14**, 2781–2804 (2003)
25. A. Geiss, H.M. Vahrenkamp, Inorg. Chem. **39**(18), 4029–4036 (2000)
26. M.M. Maľarová, J. Černák, M. Matik, J. Briančin, F. Varret, J. Therm. Anal. Cal. **136**(2), 703–715 (2019)
27. R. Bikas, V. Lippolis, N. Noshiranzadeh, H. Farzaneh-Bonab, A.J. Blake, M. Siczek, Eur. J. Inorg. Chem. **2017**(6), 999–1006 (2017)
28. B. Nowicka, T. Korzeniak, O. Stefańczyk, D. Pinkowicz, S. Chorąży, R. Podgajny, Coord. Chem. Rev. **256**(17–18), 1946–1971 (2012)
29. E. Colacio, M. Ghazi, H. Stoeckli-Evans, F. Llret, J.M. Moreno, C. Pérez, Inorg. Chem. **40**(19), 4876–4883 (2001)
30. J.J. Alexander, H.B. Gray, JACS. **90**(16), 4260–4271 (1968)
31. L.M. Siperko, T. Kuwana, Electrochim. Acta **32**(5), 765–771 (1987)
32. J. Wu, J. Song, K. Dai, Z. Zhuo, L.A. Wray, G. Liu, Z. Shen, R. Zeng, Y. Lu, W. Yang, JACS. **139**(50), 18358–18364 (2017)
33. H. Miyasaka, H. Takahashi, T. Madanbashi, K.İ Sugiura, R. Clérac, H. Nojiri, Inorg. Chem. **44**(17), 5969–5971 (2005)
34. R. Tiron, W. Wernsdorfer, F. Tuyeras, A. Scuiller, V. Marvaud, M. Verdaguer, Polyhedron **22**(14–17), 2427–2433 (2003)
35. D. Karaağaç, G.S. Kürkçüoğlu, O.Z. Yeşilel, T. Hökelek, Y. Süzen, Inorg. Chim. Acta **406**, 73–80 (2013)
36. T. Neumann, L.S. Germann, I. Moudrakovski, R.E. Dinnebier, C. dos Santos Cunha, H. Terraschke, C. Nather, Z. Anorg. Allg. Chem. **643**(23), 1904–1912 (2017)
37. J.H. Li, L. Wei, Z.Z. Bao, G.M. Wang, Z.H. Wang, Solid-State Sci. **51**, 13–17 (2016)
38. C. Krebs, I. Jess, C. Näther, Acta Crystallogr. Sect. E **77**(8), 765–769 (2021)
39. B. Beebeejaun-Boodoo, M. Rademeyer, Polyhedron **179**, 114364 (2020)
40. G.S. Kürkçüoğlu, O.Z. Yeşilel, E. Sayın, E. Enönlü, O. Şahin, J. Mol. Struct. **1219**, 128462 (2020)
41. E. Sayın, G.S. Kürkçüoğlu, O.Z. Yeşilel, O. Şahin, Polyhedron **210**, 115535 (2021)
42. G.S. Kürkçüoğlu, O.Z. Yeşilel, S. Kekeç, O. Şahin, J. Mol. Struct. **1274**, 134540 (2023)
43. H. Ünver, Trans. Met. Chem. **43**, 641–646 (2018)
44. H. Ünver, M. Kakavand, A. Neshat. Trans. Met. Chem. 1–10 (2023)
45. G.M. Sheldrick, Acta Crystallogr. Sect. A **64**(1), 112–122 (2008)
46. G.M. Sheldrick, Acta Crystallogr. Sect. A **71**(1), 3–8 (2015)
47. A.S. Package. Bruker AXS Inc., 5465. (East Cheryl Parkway, Madison, Wisconsin, USA, 2005)
48. C.F. Macrae, I. Sovago, S.J. Cottrell, P.T. Galek, P. McCabe, E. Pidcock, J. Appl. Crystallogr. **53**(1), 226–235 (2020)
49. L.J. Farrugia, J. Appl. Crystallogr. **45**(4), 849–854 (2012)
50. A. Singh, B. Boro, A. Maji, O. Singh, S. Singh, U.P. Singh, New J. Chem. **47**(18), 8951–8959 (2023)
51. D. Karaağaç, G.S. Kürkçüoğlu, O.Z. Yeşilel, M. Taş, Polyhedron **62**, 286–292 (2013)
52. D. Karaağaç, G.S. Kürkçüoğlu, O.Z. Yeşilel, T. Hokelek, H. Dal, Z. Kristallogr. **227**(9), 639–645 (2012)
53. K. Nakamoto, *Infrared and Raman Spectra of Inorganic and Coordination Compounds, Part B*, 6th edn. (Wiley, New York, 2009)
54. M.K. Krawczyk, R. Bikas, M.S. Krawczyk, T. Lis, J. Organomet. Chem. **908**, 121065 (2020)
55. M.K. Krawczyk, R. Bikas, M.S. Krawczyk, T. Lis, CrystEngComm **19**(23), 3138–3144 (2017)
56. S. Tanase, J. Reedijk. Coord. Chem. Rev. **250**(19–20), 2501–2510 (2006)
57. Y. Yu, B. Lu, X. Wang, J. Zhao, X. Wang, Q. Cai, Chem. Eng. J. **162**(2), 738–742 (2010)
58. Y. Zhou, J. Song, S. Liang, S. Hu, H. Liu, T. Jiang, J. Mol. Catal. A **308**(1–2), 68–72 (2009)
59. R. Bikas, E. Shahmoradi, N. Noshiranzadeh, M. Emami, S. Reinoso, Inorg. Chim. Acta **466**, 100–109 (2017)
60. N. Noshiranzadeh, R. Bikas, K. Ślepokura, M. Mayeli, T. Lis, Inorg. Chim. Acta **421**, 176–182 (2014)

61. N. Heydari, R. Bikas, M. Shaterian, T. Lis, Appl. Organomet. Chem. **37**(2), 6939 (2023)
62. S.C. Chen, S.N. Lu, F. Tian, N. Li, H.Y. Qian, A.J. Cui, Catal. Commun. **95**, 6–11 (2017)
63. B.R. Kim, J.S. Oh, J. Kim, C.Y. Lee, Bull. Korean Chem. Soc. **36**(12), 2799–2800 (2015)